AGU PUBLICATIONS

JGR

Journal of Geophysical Research: Oceans

RESEARCH ARTICLE

10.1002/2015JC010920

Tilt of mean sea level along the Pacific coasts of North America and Japan

Hongyang Lin[1], Keith R. Thompson[2], Jianliang Huang[3], and Marc Véronneau[3]

[1]State Key Laboratory of Marine Environmental Science, College of Ocean and Earth Sciences, Xiamen University, Xiamen, China, [2]Department of Oceanography, Dalhousie University, Halifax, Nova Scotia, Canada, [3]Canadian Geodetic Survey, SGB, Natural Resources Canada, Ottawa, Ontario, Canada

Key Points:
- Geodetic and ocean methods give similar estimates of alongshore sea level tilt
- Alongshore wind stress is main driver along the Pacific coast of North America
- The Kuroshio is the main driver along the south coast of Japan

Correspondence to:
K. R. Thompson,
keith.thompson@dal.ca

Citation:
Lin, H., K. R. Thompson, J. Huang, and M. Véronneau (2015), Tilt of mean sea level along the Pacific coasts of North America and Japan, *J. Geophys. Res. Oceans*, *120*, 6815–6828, doi:10.1002/2015JC010920.

Received 20 APR 2015
Accepted 22 SEP 2015
Accepted article online 24 SEP 2015
Published online 20 OCT 2015

Abstract The tilt of coastal mean sea level with respect to an equipotential surface is estimated using two fundamentally different approaches. The geodetic approach is based on tide gauge and GPS observations, and a model of the geoid. The ocean approach uses a high-resolution, dynamically based ocean model to estimate mean dynamic topography. Along the Pacific coast of North America the two approaches give similar large-scale profiles with a minimum at about 40°N and a maximum in the northern part of the Gulf of Alaska. Along the Pacific coast of Japan the geodetically determined coastal sea levels indicate an eastward drop of about 20 cm along the south coast and a further northward drop across Tsugaru Strait. Both of these features are reproduced by the ocean models. An analysis of the alongshore momentum balance suggests that alongshore wind stress acting over the inner shelf is the primary driver of the mean sea level profile along the coast of North America. Several large-scale features are explained using arrested topographic wave theory. A similar momentum analysis, and an additional study of time variability of sea level and circulation, suggests that the Kuroshio is the main driver of the mean sea level tilt along the south coast of Japan. Discrepancies in the alongshore tilt of sea level estimated by the geodetic and ocean approaches along both coasts are discussed in terms of errors in the ocean and geoid models.

1. Introduction

Coastal sea level is a geophysical variable of considerable interest to geodesists and oceanographers [e.g., *Pugh and Woodworth*, 2014]. For example, geodesists and oceanographers have, for many years, tried to reconcile differences in the mean meridional slope of coastal sea level estimated by geodetic and ocean leveling, and interest in this topic continues to the present day [e.g., *Featherstone and Filmer*, 2012; *Penna et al*., 2013, and references therein]. Oceanographers are interested in using tilts of sea level, defined with respect to the geoid, to make inferences about deep ocean and shelf circulation and also to evaluate circulation models [e.g., *Kuroishi*, 2013; *Higginson et al*., 2015]. Climatologists are using long records of coastal sea level to estimate changes in the rate of global sea level rise and the frequency of occurrence of extreme sea level events [e.g., *Menéndez and Woodworth*, 2010].

Spatial gradients of mean sea level in the deep ocean are, to first order, in geostrophic balance with the surface flow just below the wind-driven Ekman layer [e.g., *Pedlosky*, 1987]. This balance does not hold at the coast because the flow perpendicular to the coastline is zero. This means that the physics controlling the circulation and the tilts of sea level are fundamentally different near the coast. For example, *Csanady* [1978] has shown that an alongshore wind blowing over a portion of the shelf can influence the coastal tilt of sea level hundreds of kilometers "downstream" in the sense of coastal trapped wave propagation. Another consequence of the coastal boundary condition is that small wavelength variations of sea level on the shelf are not seen in coastal sea level [*Csanady*, 1982]. Steep bathymetric gradients of the continental slope can also suppress small-scale variability in the deep ocean, allowing only those signals with length scales of thousands of kilometers to be detected at the coast [e.g., Huthnance, 2004]. In summary, the alongshore momentum balance along the coast is quite subtle and has to be taken into account when, for example, using coastal sea level to evaluate ocean models, and also downscale projections of sea level rise from the deep ocean models to the coast [*Higginson et al*., 2015].

In a recent study of sea level along both coasts of the Atlantic, and the east coast of the Pacific, *Woodworth et al*. [2012] estimated the alongshore variation of coastal mean sea level using two fundamentally different

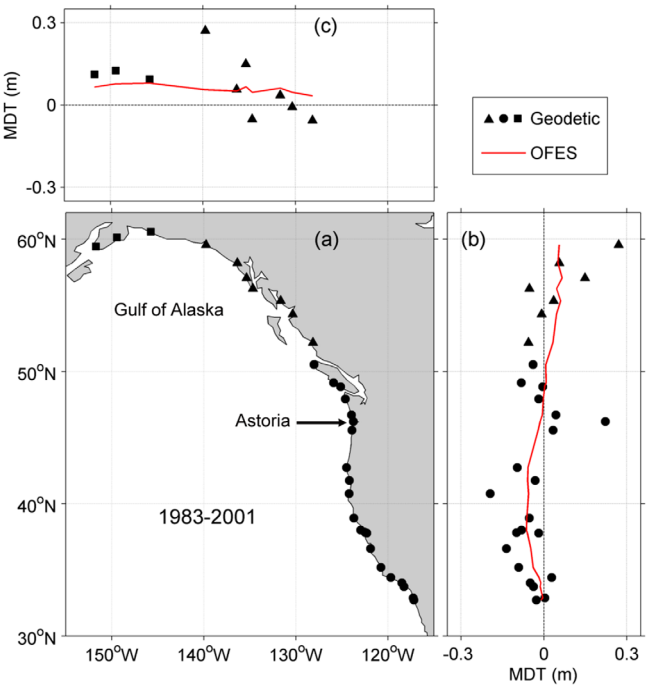

Figure 1. Coastal mean sea level for North America estimated using the geodetic and ocean approaches. (a) Locations of the 31 tide gauges. (b) Geodetically determined sea level at tide gauges as a function of latitude (symbols). Predictions by the OFES model are shown by the red line. (c) Same as Figure 1b except as a function of longitude and for gauges near, and around, the Gulf of Alaska. Tide gauges common to the latitude and longitude plots are shown as triangles. The spatial mean of each profile has been removed. The averaging period is 1983–2001 for the geodetic estimates and 1993–2001 for the ocean (OFES) estimates. Changing the ocean model averaging period to 1983–2001 causes differences of less than 1 cm at all gauges.

approaches. The "geodetic approach" is based on a geoid model and sea level observations that have been referenced using GPS measurements and leveling of tide gauge benchmarks. The "ocean approach" uses the sea surface topography defined with respect to the geoid (henceforth the mean dynamic topography, MDT) calculated directly by a high-resolution ocean model. *Woodworth et al.* [2012] found an encouraging level of agreement between the two approaches, thereby providing some validation of the recent generation of geoid and ocean models.

More recently, *Higginson et al.* [2015] examined the tilt of mean sea level along the east coast of North America using 7 geoid models and 11 ocean models (all with horizontal grid spacing less than 1°). By focusing attention on only those geoid models using terrestrial gravity data, *Higginson et al.* [2015] found that the standard deviation of the differences of the means of the geodetic estimates and the corresponding means of the ocean estimates was only 2.3 cm.

In the present study, the geodetic and ocean approaches are used to estimate the alongshore profiles of mean sea level along the Pacific coasts of North America and Japan. Our analysis extends the study of *Woodworth et al.* [2012] in the sense that it includes more tide gauges in the Gulf of Alaska and 13 new tide gauges along the coast of Japan. The present study uses two regional geoid models: JGEOID2008 [*Kuroishi and Keller*, 2005; *Kuroishi*, 2009] for the coast of Japan and CGG2013 [*Huang and Véronneau*, 2013] for the Pacific coast of North America. These regional geoid models are preferred over EGM2008 [*Pavlis et al.*, 2012, 2013] because they use higher-resolution gravity and terrain data and this can lead to a reduction in the omission error. The present study also uses output from two ocean models: the Community Earth System Model (CESM) [*Small et al.*, 2014] and the Oceanic General Circulation Model for the Earth Simulator (OFES) [*Sasaki et al.*, 2008]. After showing generally good agreement between the alongshore tilts of MDT predicted by the geodetic and ocean approaches, the alongshore momentum balance near the coast is used to physically interpret the alongshore tilts using output from the OFES model.

The structure of the paper is as follows. The two independent approaches used to estimate the coastal tilt of MDT are described in section 2. Mean profiles along the coasts of North America and Japan are described in section 3 and they are physically interpreted in section 4. Results are summarized and discussed in section 5.

2. Data and Methods

2.1. Geodetic Approach

The locations of 31 tide gauges along the coast of North America are shown in Figure 1a. The station names, latitudes, and longitudes are listed in Table 1. This set of tide gauges was chosen according to three criteria:

Table 1. Mean Dynamic Topography (in m) at the 31 Tide Gauges Along the Pacific Coast of North America Calculated by the Geodetic and Ocean Approaches[a]

Station	°N	°W	Geodetic[b]	Ocean[c]
San Diego	32.714	117.174	−0.027	−0.010
La Jolla	32.867	117.258	0.004	−0.004
Los Angeles	33.720	118.272	−0.038	−0.013
Santa Monica	34.008	118.500	−0.050	−0.011
Santa Barbara	34.408	119.685	0.028	−0.017
Port San Luis	35.177	120.760	−0.091	−0.038
Monterey	36.605	121.888	−0.136	−0.047
Alameda	37.772	122.298	−0.019	−0.060
San Francisco	37.807	122.465	−0.099	−0.060
Point Reyes	37.996	122.977	−0.081	−0.063
Arena Cove	38.913	123.708	−0.053	−0.062
North Spit	40.767	124.217	−0.195	−0.055
Crescent City	41.745	124.183	−0.032	−0.059
Port Orford	42.739	124.498	−0.096	−0.057
Garibaldi	45.554	123.919	0.033	−0.021
Astoria	46.207	123.768	0.223	−0.014
Toke Point	46.708	123.967	0.043	−0.005
La Push	47.913	124.637	−0.019	−0.002
Bamfield	48.840	125.140	−0.004	0.003
Tofino	49.150	125.910	−0.082	0.008
Winter Harbour	50.510	128.030	−0.039	0.007
Bella Bella	52.160	128.140	−0.056	0.033
Prince Rupert	54.320	130.320	−0.008	0.046
Ketchikan	55.332	131.626	0.036	0.061
Port Alexander	56.247	134.647	−0.052	0.046
Sitka	57.052	135.342	0.150	0.066
Elfin Cove	58.195	136.347	0.057	0.051
Yakutat	59.548	139.733	0.271	0.056
Cordova	60.558	145.753	0.094	0.079
Seward	60.120	149.427	0.126	0.077
Seldovia	59.441	151.720	0.112	0.065

[a]The inverse barometer correction has been made to the geodetic estimates. The means of columns 4 and 5 have been removed.
[b]Sea levels for the Canadian and US tide gauges obtained from the Canadian Hydrographic Service and National Geodetic Survey, respectively. The CGG2013 geoid was used.
[c]Based on OFES model averaged over the period of 1993–2001.

(i) exposure to the open ocean, (ii) availability of a relatively long (at least 5 years) sea level record, and (iii) good spatial coverage and roughly equal spacing of tide gauges along the coast.

The US National Geodetic Survey provided the US tide gauge data in the form of mean sea levels averaged over the period of 1983–2001 with respect to the GRS80 ellipsoid in the North American Datum of 1983 (NAD83) reference frame. The data were transformed to the International Terrestrial Reference Frame (ITRF) 2010.

The data for the five Canadian gauges were provided by Fisheries and Oceans Canada in the form of monthly sea levels and benchmark elevations with respect to chart datum. Natural Resources Canada averaged the monthly data over the period of 1993–2011 and calculated the averaged sea levels with respect to the GRS80 ellipsoid. The ITRF2010 ellipsoidal heights of the tide gauge benchmarks were adjusted to the midpoint of the averaging period of the sea level observations using the vertical velocity model of *Craymer et al*. [2011]. Two approaches were subsequently used to correct the Canadian data for the 10 year difference in their epoch (2002) and that of the US data (1992). First, we used the trend of absolute sea level of 0.74 mm per year estimated by *Santamaría-Gómez et al*. [2012] for this region (see row labeled NW North America in their Table 1). This estimate is based on trends in relative sea level and colocated GPS measurements. The net effect is an overall reduction in the Canadian levels of 0.74 cm. The second approach uses the vertical velocities of *Craymer et al*. [2011] and observed trends in relative mean sea level for each of the five Canadian gauges. (All available annual means for the period of 1973–2014 were obtained from the Permanent Service for Mean Sea Level (PSMSL) [*Woodworth and Player*, 2003] to estimate the trends.) We found site-specific reductions between 1.0 and 2.9 cm. In this study we use the approach based on the trend of absolute sea level estimated by *Santamaría-Gómez et al*. [2012].

The Canadian Gravimetric Geoid model (CGG2013) was used for the Pacific coast of North America. It is defined on a grid with a spacing of $1/30^{\circ}$. CGG2013 was developed following the same procedure as for CGG2010 [*Huang and Véronneau*, 2013] with two exceptions: (1) the underlying model is EIGEN6C3stat [*Förste et al*., 2013] to spherical harmonic degree and order 120 and with weight from 1 to 0 from degree 120 to 180; and (2) the marine altimetry-derived gravity data are from the DTU10 model [*Andersen et al*., 2010; *Andersen*, 2010]. The estimated standard deviations of the geoid errors at the 31 tide gauges range from 1.6 to 5.9 cm and have a median of 2.9 cm. Comparison of CGG2013 geoid undulations with independent GPS/leveling measurements made at 72 benchmarks on Vancouver Island gives an error standard deviation of 4.4 cm.

The locations of the 13 tide gauges along the Pacific coast of Japan are shown in Figure 2a and listed in Table 2. This set of tide gauges was chosen based on the three criteria given above and also the availability of GPS data and ocean model output. All available monthly mean sea levels for the period of 2003–2007 were obtained from the PSMSL. The data were defined with respect to their Revised Local Reference (RLR).

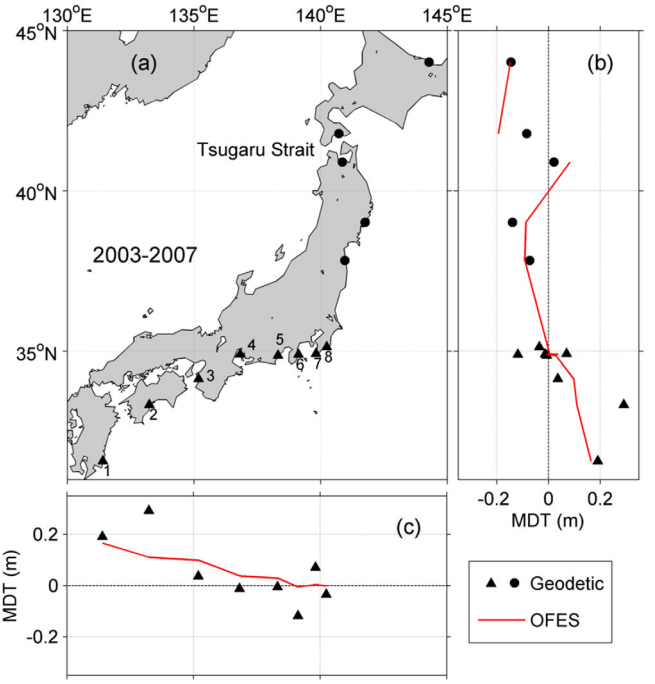

Figure 2. Coastal mean sea level for the coast of Japan. Same as Figure 1 except for the break in the red line indicating Tsugaru Strait. The averaging period is 2003–2007 for both approaches.

GPS data for the local benchmarks of the Japanese tide gauges were obtained from the Systeme d'Observation du Niveau des Eaux Littorales (SONEL, http://www.sonel.org/). SONEL provides a constant vertical offset between the GPS benchmark and the RLR of each tide gauge, and a weekly time series of GPS benchmark heights relative to the GRS80 ellipsoid which can vary due to vertical land motion [*Santamaría-Gómez et al.*, 2012]. In order to take vertical land motion into account, the monthly PSMSL time series were linearly interpolated to weekly values in order to align them with the GPS data. Note station Kushiro (144.371°E, 42.976°N) was omitted because of a large offset in the GPS time series provided by SONEL.

The time mean of sea level with respect to the geoid was calculated using the latest version of the Japanese geoid model, JGEOID2008 [*Kuroishi and Keller*, 2005; *Kuroishi*, 2009]. This model covers the ocean areas around Japan and is based on GRACE (Gravity Recovery and Climate Experiment), surface (land and ship-borne), and altimetry-derived marine data. The output is provided on a 1/60° by 1/40° grid relative to the GRS80 ellipsoid. Comparison with independent height estimates based on GPS and leveling at 816 benchmarks gives residuals with a standard deviation of 8.4 cm. *Kuroishi* [2013] notes JGEOID2008 is slightly better than EGM2008 for Japan. Initially, we included the tide gauge at Kushimoto (33.48°N, 135.77°E). However, JGEOID2008 contains systematic errors in the vicinity of this gauge [*Kuroishi*, 2013] and so it was excluded from the present analysis.

Table 2. Mean Dynamic Topography (in m) at the 13 Tide Gauges Along the Pacific Coast of Japan Calculated by the Geodetic and Ocean Approaches[a]

Station	°N	°E	Geodetic[b]	Ocean[c]
Aburatsu	31.577	131.409	0.218	0.165
Kure	33.334	133.243	0.293	0.110
Kainan	34.144	135.191	0.055	0.099
Onisaki	34.904	136.824	−0.003	0.037
Yaizu	34.871	138.327	−0.011	0.029
Ito	34.896	139.133	−0.115	−0.006
Mera	34.919	139.825	0.061	0.004
Katsuura	35.129	140.249	−0.043	−0.002
Soma	37.831	140.962	−0.066	−0.092
Ofunato	39.020	141.753	−0.138	−0.087
Asamushi	40.898	140.859	0.008	0.083
Hakodate	41.782	140.725	−0.094	−0.194
Abashiri	44.019	144.286	−0.165	−0.147

[a]The inverse barometer correction has been made to the geodetic estimates. The means of columns 4 and 5 have been removed.
[b]Sea levels for the tide gauges were obtained from PSMSL in the form of monthly means defined with respect to their Revised Local Reference. The JGEOID2008 geoid model was used.
[c]Based on OFES model averaged over the period of 2003–2007.

The procedure used to estimate the MDT from the tide gauge and GPS data and the geoid model is described by *Woodworth et al.* [2012]. All heights for both coasts were defined in the mean tide system using the formulae given by *Ekman* [1989]. The inverse barometer correction was made to the mean sea level profiles along each coastline using sea level pressure fields obtained from the National Centers for Environmental Prediction (NCEP) Climate Forecast System Reanalysis [*Saha et al.*, 2010].

2.2. Ocean Approach

The output from two high-resolution, global ocean models has been used to estimate MDT. The CESM ocean model uses a tripole grid with poles located over land (North America and Asia). The grid spacing is, on average, 0.1° and decreases from 11 km at the Equator to 2.5 km at high latitudes [*Small et al.*, 2014]. Output from a 48 year run of this model was kindly made available by Dr Yu-heng Tseng. The

Table 3. Differences (in cm) of Sea Level Along the Pacific Coasts of Japan and North America Predicted by the Two Ocean Models[a]

Coast	Model	μ_Δ	σ_Δ (m = 5)	σ_Δ (m = 10)
Japan	CESM	34.8	3.3	2.4
	OFES	30.3	1.7	1.2
North America	CESM	−12.0	1.4	1.1
	OFES	−11.7	1.1	0.7

[a]For the coast of Japan the sea level difference is between the most southerly and northerly tide gauge (Table 2). For the North American coast the sea level difference is between North Split (40.8° N) and Seldovia (59.4° N, Table 1). The column labeled μ_Δ is the difference of the long-term means at the two tide gauges computed from the complete model runs (48 years for CESM, 62 years for OFES). The last two columns show the standard deviation of the time-varying difference after applying an m = 5 and m = 10 year running mean.

OFES model has a grid spacing of 0.1° and output was obtained from the Earth Simulator Center of the Japan Agency for Marine-Earth Science and Technology (JAMSTEC) [*Sasaki et al.*, 2008] for the period of 1950–2011. Neither model assimilates observations.

Time series of sea level computed at the nearest valid "wet" grid point to each tide gauge were extracted from both sets of model output. Given the irregular shape of the coastal boundary, and the proximity of land points at which the MDT is not defined, this is the least error-prone and most direct form of spatial interpolation.

According to CESM and OFES, mean sea level drops by 35 and 30 cm, respectively, moving east, and then north, along the coast of Japan (Table 3). The standard deviation of the time-varying drop, after applying a 5 year running mean to each time series, is 3 and 2 cm for CESM and OFES, respectively (Table 3). Along the North American coast, both models agree that mean sea level increases by 12 cm from 40.8°N and 59.4°N and the standard deviation of the time-varying difference is 1 cm after applying a 5 year running mean. Based on these results we conclude that the mean sea level profiles estimated by the two models are similar on the large scale, and stable through time for averaging periods of 5 years and longer.

3. Results

3.1. North America

The geodetically determined values of MDT at the 31 tide gauges have a standard deviation of 10.1 cm (Table 4). The autocorrelation of the alongshore profile (Figure 3) has a "jump" in autocorrelation at zero lag. This suggests the MDT profile can be decomposed into a larger-scale signal and a "white noise" component that varies independently from gauge to gauge. Based on the extrapolation of the autocorrelation to zero lag [*Daley*, 1993], the standard deviation of the noise and large-scale signals are estimated to be 7.6 and 6.7 cm, respectively. The large-scale signal has the following characteristics (Figure 1): (i) roughly equal mean sea levels in the vicinity of 32°N and 50°N with a minimum, about 10 cm lower, at about 40°N; (ii) an increase of about 20 cm moving northward from the minimum into, and around, the Gulf of Alaska. (Note the outlier at 46.2°N is for the Astoria tide gauge which is located close to the mouth of Columbia River.)

The coastal profile of mean sea level predicted by the OFES model is smoother (Figures 1b and 1c) and less variable (Table 4) than the geodetic estimates. The ocean model reproduces the large-scale characteristics of the geodetic profile defined by (i) and (ii) above although the range in heights is about 25% lower (Table 1). The correlation between the geodetic and OFES profiles is 0.63 and the standard deviation of their difference is 8.0 cm (Table 4). Applying a running median of length 3 to the geodetic estimates to suppress the small-scale variability increases the correlation to 0.81 and decreases the standard deviation of the differences to 4.3 cm. *Woodworth et al.* [2012] also calculated the standard deviation of the difference between ocean and geodetic estimates for the period of 1993–2002 at 26 tide gauge locations and found a standard deviation of 13.7 cm. One reason for the larger standard deviation found by *Woodworth et al.* [2012] is that they used GOCO03S which is a purely satellite-derived geoid model. Its commission error increases rapidly at higher degrees and its omission error is higher than

Table 4. Standard Deviation (in cm) of Profiles of MDT Along the Pacific Coasts of Japan and North America[a]

Coast	σ_G	σ_O	σ_{G-O}	$\rho_{G,O}$
North America	10.1	4.7	8.0	0.63
Japan	13.4	10.5	8.0	0.80

[a]The column labeled σ_G is the standard deviation of the geodetic profile. The column labeled σ_O is the standard deviation of the ocean model (OFES) profile interpolated to the tide gauges. The last two columns give the standard deviation of the difference, and the correlation, of the geodetic and ocean profiles.

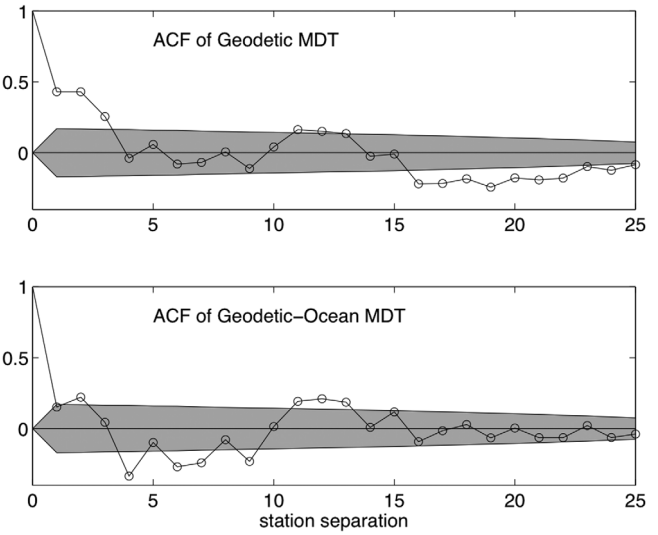

Figure 3. Spatial autocorrelation of the geodetic profile along the coast of North America. For simplicity it is assumed the separation between adjacent stations is constant. (top) Geodetic profile and (bottom) difference between the geodetic and ocean estimates shown in Figure 1. The shaded region indicates the statistical significance of the autocorrelations. It is defined by ±one standard deviation of an ensemble of sample autocorrelations functions calculated from 10^4 realizations of white noise time series of length 31 (the number of tide gauges).

the combined satellite/terrestrial geoid models used in the present study.

Figure 3 (bottom) shows the autocorrelation of the geodetic profile after removal of the OFES predictions. The autocorrelations for nonzero lags are reduced overall and consistent with differences that are approximately uncorrelated from gauge to gauge.

3.2. Japan

The 13 geodetically estimated mean sea levels have a standard deviation of 13.4 cm (Table 4). Most of the change occurs along the south coast of Japan, between tide gauges 1 and 8 near the Kuroshio separation point (Figure 2a). A northward sea level drop of 12 cm is also evident across Tsugaru Strait (Table 1). This implies a mean surface geostrophic current flowing from the Sea of Japan to the Pacific, consistent with current meter observations [e.g., *Ito et al.*, 2003].

The ocean and geodetic estimates of MDT are generally in good agreement (Figures 2b and 2c). Both estimates indicate an eastward drop of about 20 cm along the south coast of Japan and an additional northward drop across Tsugaru Strait. More quantitatively, the correlation between the geodetic and ocean profiles is 0.80 and the standard deviation of their difference is 8.0 cm (Table 4).

4. Dynamical Interpretation

4.1. Background and Approach

The alongshore component of the time and depth-averaged horizontal momentum equation close to shore is taken to be [e.g., *Csanady*, 1982]:

$$g\frac{\partial \eta}{\partial s} = \frac{\tau^s}{\rho_0 h} + F^s - \frac{g}{h}\int_{-h}^{0}(z+h)\frac{\partial \epsilon}{\partial s}\,dz, \tag{1}$$

where g is the acceleration due to gravity (assumed constant), η denotes sea level after correction for the inverse barometer effect, s is the alongshore coordinate, h is water depth, τ^s is the alongshore component of wind stress, F^s is the alongshore component of friction, and $\epsilon=(\rho-\rho_0)/\rho_0$ where ρ_0 is a fixed reference density.

Several terms that are important in deeper water have been dropped in order to arrive at (1). The coastal boundary condition of no-normal flow means that the Coriolis term makes a vanishingly small contribution as the coast is approached. The horizontal advection term is generally small in comparison to the bottom friction term because the latter is inversely proportional to h which is usually small close to shore.

The contribution of horizontal changes of water density is given by the last term in (1). As the coast is approached the water depth usually (but not always) approaches zero and, under such circumstances, the density term will make a negligible contribution to the alongshore momentum balance. We have retained the density term because model depth is not always small at the coast.

In accord with earlier studies [e.g., *Csanady*, 1982; *Xu and Oey*, 2011; *Higginson et al.*, 2015] we use (1) to estimate, and interpret, the variation of MDT along the Pacific coasts of Japan and North America.

The alongshore component of friction, F^s, is assumed to be the sum of contributions from bottom and horizontal friction, denoted by F_b^s and F_h^s, respectively. Observations suggest that F^s is dominated by F_b^s in shallow water [e.g., *Csanady*, 1982]. Bottom stress is usually modeled using a quadratic drag formulation (OFES uses such a formulation). Following the approach of *Wright and Thompson* [1983] to approximate the time mean of bottom stress, we assume

$$F_b^s = -\frac{c_d}{h}\left(v_b^2 + 4\sigma^2\right)^{1/2} v_b, \tag{2}$$

where c_d is the drag coefficient, v_b is the mean alongshore flow, and σ is the standard deviation of the time-varying currents.

Both of the ocean models discussed in this study include horizontal friction, F_h^s [*Pacanowski and Griffies*, 1998]. This means that the model's flow, and thus the bottom stress term F_b^s, will be zero at the coast. It is important to note however that both models use relatively weak biharmonic friction. This implies that the effect of horizontal friction will be confined to narrow frictional sublayers that bring the velocity (and bottom stress) to zero as the coast is approached while leaving the total stress F^s unchanged, i.e., as F_b^s drops to zero, F_h^s will increase to keep F^s approximately constant. (A similar situation arises in studies of western intensification of ocean circulation: if a "Stommel layer", dependent on bottom friction, is augmented by a narrow "Munk sublayer", dependent on horizontal friction, in order to satisfy no-slip at the coast [*Pedlosky*, 1987], there is no change in F^s over the Munk sublayer.) The reason it is important to consider F_h^s in the present study is that F_b^s is calculated one grid point away from the coast and it is therefore likely that F_b^s will have been reduced by the inclusion of horizontal friction.

In the following sections 4.2 and 4.3, we integrate the individual terms on the right-hand side of (1) along the coast and thereby diagnose the contributions of alongshore wind stress (η^τ), bottom friction (η^{F_b}), and density (η^d) to the alongshore variation of coastal sea level:

$$\eta(s) = \eta^\tau(s) + \eta^{F_b}(s) + \eta^d(s). \tag{3}$$

A major advantage of focusing on these sea level components, rather than the individual terms in the alongshore momentum equation (1), is that the integration smooths out the effect of small-scale variations in bathymetry and coastline orientation, leading to results that are easier to visualize and interpret.

The only explicit forcing term in (1) is the alongshore wind stress, τ^s. It is possible however for other types of forcing to drive an alongshore tilt of sea level if they change the alongshore flow, and thus F^s. For example, a prescribed sea level variation along the shelf break will be associated with geostrophically balanced, cross shelf surface flows that can drive currents, and thus tilts of sea level, along the coast [e.g., *Huthnance*, 2004]. Similarly, spatial changes in the density over the shelf, due for example to the terrestrial input of freshwater, can also drive nearshore currents and tilts of sea level along the coast [*Csanady*, 1982].

4.2. North America

Mean wind stress over the shelf seas bordering the eastern North Pacific is predominantly along shelf (Figure 4a) and has a typical magnitude of 0.1 Pa. (The wind stress fields used in this study came from the NCEP/NCAR (National Center for Atmospheric Research) reanalysis [*Kalnay et al.*, 1996]. The same fields were used to drive the OFES model [*Sasaki et al.*, 2008]. They were provided by JAMSTEC, together with the ocean model output.) Wind stress is weak in the vicinity of 42°N and generally has a poleward component north of this latitude, and an equatorward component south of it. The distribution of mean surface currents over the shelf (Figure 4b) is qualitatively similar to that of the wind but the region of near-zero current speed is farther north, centered on about 48°N. The mean sea level distribution over the shelf indicates strong cross-shelf gradients with sea level changes of order 10 cm (Figure 4c). These gradients are associated with geostrophically balanced, alongshelf surface currents of order 10 cm s^{-1}. Sea level changes of order 10 cm are also predicted along the coast (see red line in Figure 1) but the changes occur on much larger scales (thousands of kilometers) as discussed above. The minimum in coastal sea level occurs at about 38°N (Figure 1).

Equation (1) holds in water shallower than about 20 m [e.g., *Csanady*, 1982]. The shelf off southern California (30°N–37°N) is narrow and more than 15% of the wet points closest to the coast in the OFES model have depths exceeding 200 m. We therefore started the alongshore integration of (1) at about 37°N. (See blue

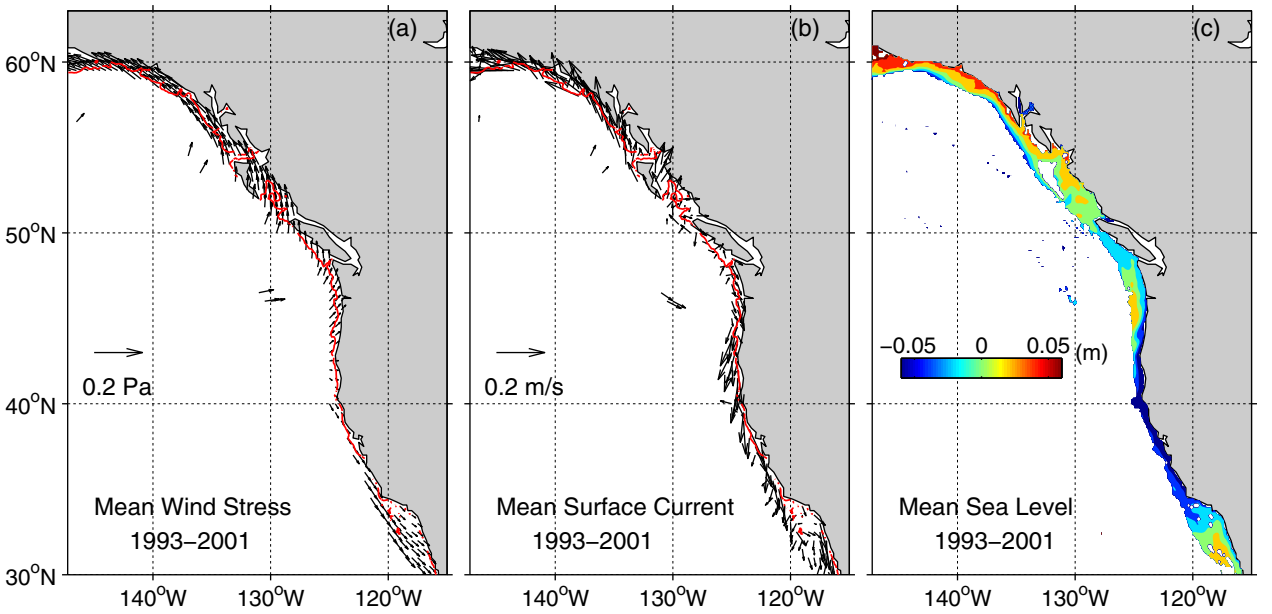

Figure 4. Annual means of (a) wind stress, (b) surface current, and (c) sea level over the shelf (depths <2000 m) of the eastern North Pacific based on OFES model forcing and output for the period of 1993–2001. The red lines in Figures 4a and 4b denote the 200 m isobath.

line Figure 5a. Along this stretch of coast less than 2% of the coastal wet points have depths exceeding 200 m.)

The contribution of the wind (η^{τ}, obtained by alongshore integration of $\tau^{s}/\rho_0 gh$ evaluated at the nearest velocity point to the model coastline) has a range of about 60 cm (red line, Figure 5). The wind contribution increases toward northward (southward) for latitudes greater (less) than about 42°N, in accord with the above description of the wind stress over the shelf.

The contribution of bottom stress, η^{F_b}, was obtained by integrating F_b^s alongshore. The bottom drag coefficient was taken to be $c_d = 0.0025$, in agreement with the value used by OFES. The standard deviation of the

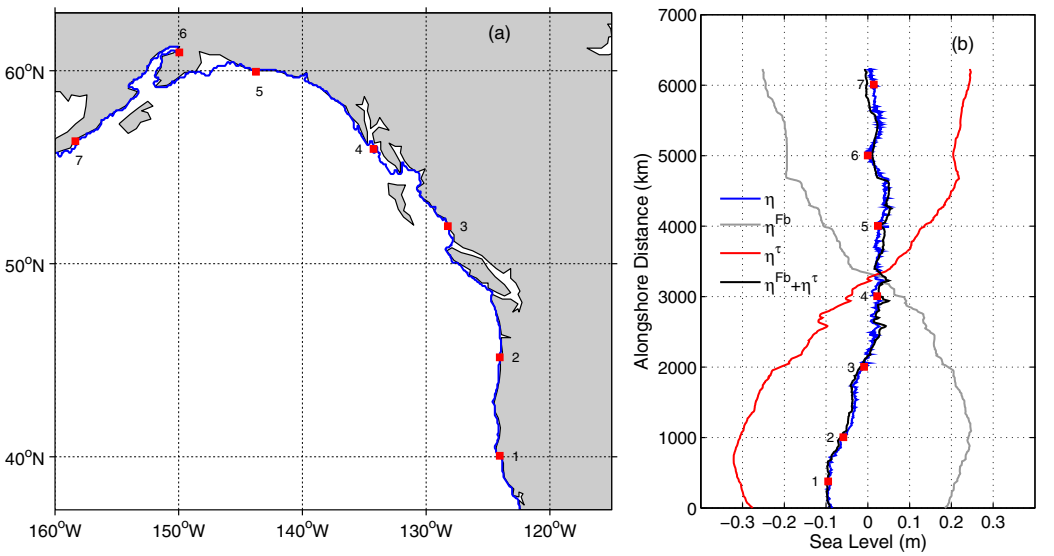

Figure 5. Momentum balance along the Pacific coast of North America. (a) The integration path along the coast is shown by the blue line. The red squares are arbitrarily chosen markers along the coast. (b) Sea level components calculated from OFES model output using (3). The blue line denotes sea level calculated directly by the model. The red and gray lines show sea level contributions from wind stress and bottom friction; the black line shows their sum. Spatial means of all lines were removed prior to plotting.

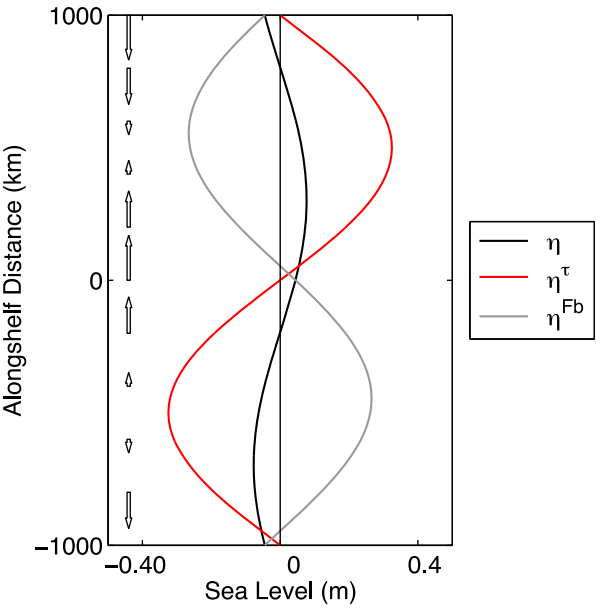

Figure 6. Alongshore variation of sea level according to the idealized arrested topographic wave model described in the text. The coast is aligned with the *y* axis and the bathymetry depends only on offshore distance. The model is forced by an alongshore wind that is periodic in *y*. All model parameters are given in the text. The black line shows the sea level variation at the coast. The red and gray lines show the contributions of alongshore wind and bottom stress, obtained by integrating (4). Note the model is configured so that coastal trapped waves propagate in the positive *y* direction. The arrows to the left of the figure indicate the direction and strength of the alongshore wind stress.

high-frequency current variations (see equation (2)) was taken to be $\sigma = 25$ cm s^{-1}. The variations of η^{F_b} almost mirrors the changes in η^{τ} (see Figure 5, gray line), indicating that alongshore wind stress and bottom stress are in approximate balance near the coast.

The sum of wind and bottom stress contributions ($\eta^{\tau}+\eta^{F_b}$) agrees well with the profile calculated by OFES (Figure 5, compare black and blue lines); the standard deviation of their difference is only 1 cm. We also calculated the direct influence of the density field using the term η^{d} (not shown). The range of η^{d} was 6 cm, significantly smaller than the range of η^{τ} and η^{F_b}. We also found that η^{d} was largely cancelled by the effect of lateral friction and so we will ignore these terms in the discussion that follows. It is clear from Figure 5 that (i) the variation of η is small compared to η^{τ} and η^{F_b}, and (ii) the extrema of these three components occur at different latitudes. We now attempt to explain (i) and (ii) using the arrested topographic wave theory of *Csanady* [1978].

Assume an idealized, homogeneous shelf sea on an *f*-plane with an infinitely long coast aligned with the *y* axis. The water depth equals h_0 at the coast ($x = 0$) and it increases with offshore distance, i.e., $h = h_0 + \alpha x$ where α is the bottom slope. The wind stress is assumed steady, alongshore and of the form $\tau_0 \cos(ly)$ where l is the alongshore wave number. Following *Csanady* [1982], the alongshore flow is assumed to be in geostrophic balance. The depth-integrated, alongshore momentum balance is taken to be

$$fu = -g\frac{\partial \eta}{\partial y} + \frac{\tau^{y}}{\rho_0 h} - \frac{rv}{h}, \tag{4}$$

where r is a (linearized) bottom drag coefficient. Supplementing the momentum equations by (i) the continuity equation, (ii) the coastal boundary condition of no-normal flow ($u = 0$), and (iii) a far-field condition ($\eta \to 0$ as $x \to \infty$), *Csanady* [1982] showed that sea level satisfies a parabolic partial differential equation (pde) that diffuses information alongshore, in the direction of propagation of coastal trapped waves (northward along the Pacific coast of North America). According to this pde, winds blowing along the coast of southern California, for example, will affect the sea level further north due to the propagation of information along the coastal waveguide.

The coastal sea level profile, calculated using the arrested topographic wave model outlined above, is shown in Figure 6 along with η^{τ} and η^{F_b}. We assumed $f = 10^{-4}$ s^{-1}, $h_0 = 20$ m, $\alpha = 0.003$, $r = 5\times10^{-4}$ m s^{-1}, $l = 2\pi/2000$ km, and $\tau_0 = 0.2$ Pa. There is qualitative agreement between the predictions from the arrested topographic wave model and the sea level components calculated by OFES (compare Figures 5 and 6). Note the ordering of the latitudes at which η, η^{τ}, and η^{F_b} reach their extreme values, and their relative magnitudes, agree with the OFES results shown in Figure 5. Based on this agreement we conclude that the alongshore wind acting over the inner shelf is the primary driver of the mean sea level tilts along the Pacific coast of North America. This conclusion is in accord with *Hickey and Pola* [1983] who also used an arrested topographic wave model and more realistic wind forcing (but did not include a coastal wall, or split the solution into the components shown in Figure 6).

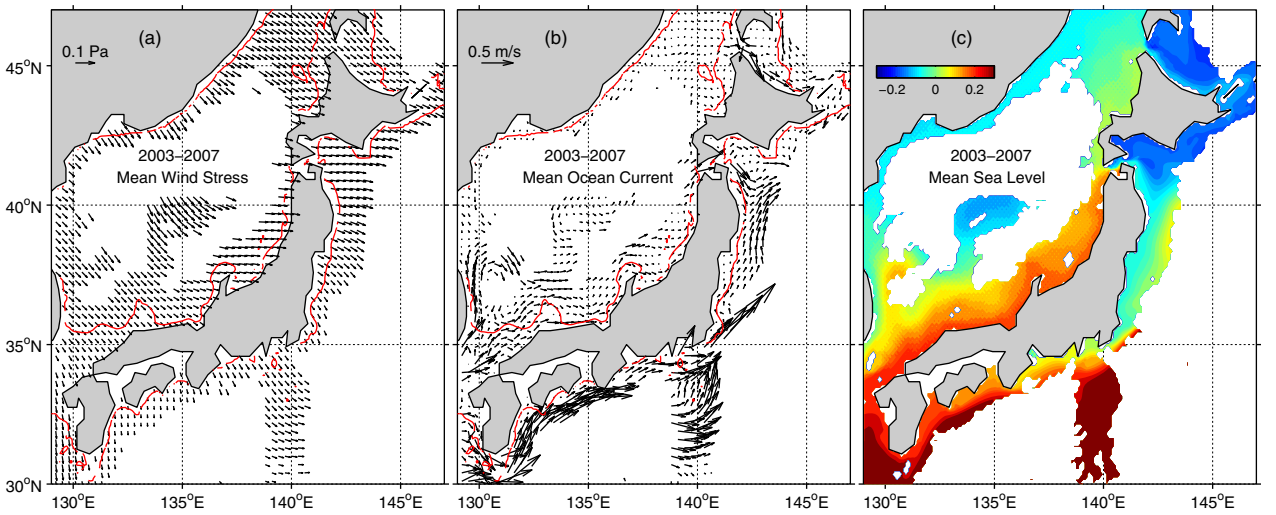

Figure 7. Annual means of (a) wind stress, (b) surface current, and (c) sea level (in m) over the Japanese shelf (depths <2000 m) based on OFES forcing and output for the period of 2003–2007. The red lines in Figures 7a and 7b denote the 200 m isobath.

4.3. Japan

Mean wind stress over the Japanese shelf bordering the North Pacific is approximately offshore (Figure 7a). The typical stress magnitude is 0.05 Pa. The mean surface currents predicted by OFES flow along the shelf to the northeast in this region (Figure 7b). Higher speeds are evident south of the Kuroshio separation point (at about 35°N), with typical speeds of 50 cm s^{-1}. This is also evident in the shallow water close to shore, implying that the Kuroshio may have an important impact on coastal circulation in this region. The MDT (Figure 7c) has a downward tilt in the same direction as the flow along the shelf. Sea level changes of order 30 cm occur along the Pacific coast of Japan (excluding Hokkaido).

The alongshore momentum equation was integrated along the coast of Japan to obtain η^{τ}, η^{F_b}, and η^{d}, as for the North American coast. The island of Hokkaido was excluded and it was assumed $\sigma = 0.4$ m s^{-1}. The

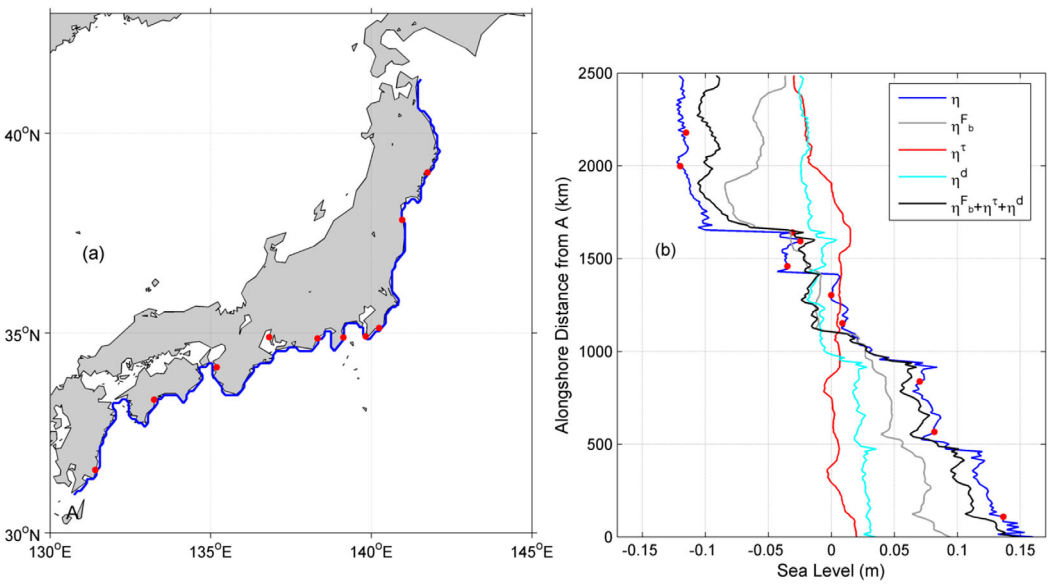

Figure 8. Momentum balance along the Pacific coast of Japan. Similar to Figure 5 but that the cyan line denotes sea level contribution due to changes in water density.

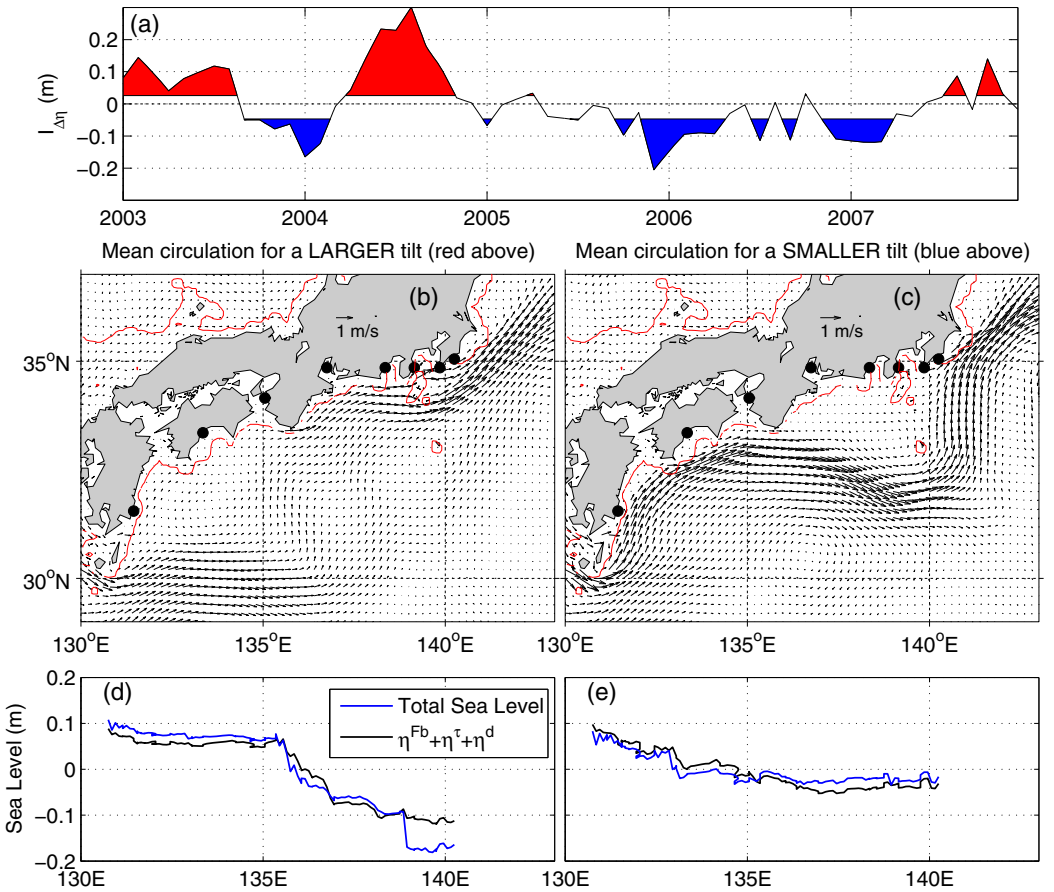

Figure 9. Mean surface circulation, and profiles of coastal sea level, conditioned on the tilt index $I_{\Delta\eta}$. All quantities were calculated from OFES output. (top) Time variation of $I_{\Delta\eta}$ (see text for details). The red (blue) shading defines times when $I_{\Delta\eta}$ is above (below) the second (first) tercile. These times are used to form the conditional means displayed in the remaining panels. (middle) Surface circulation conditioned on $I_{\Delta\eta}$. (bottom) Coastal sea level, and $\eta^{\tau}+\eta^{F_b}+\eta^{d}$, conditioned on $I_{\Delta\eta}$.

sum of these three terms closely resembles the alongshore variation of η (Figure 8b); the standard deviation of the difference is 1.8 cm. The biggest contributor to the total drop of about 27 cm is η^{F_b} (18 cm), followed by η^{d} (5 cm) and η^{τ} (4 cm). The reason η^{τ} is so small is the mean wind stress is predominantly offshore in this region as noted above. Less than 10% of the wet points close to shore have depths exceeding 200 m.

The fact that η^{F_b} approximately equals sea level at the coast raises the question of what drives the coastal circulation (leading to the bottom stress and thus changes in η^{F_b}). To answer this question we calculated the *time variation* of the tilt of sea level along the south coast of Japan and related it to regional changes in the model's circulation and density fields. The following simple index was used to calculate the time varying tilt:

$$I_{\Delta\eta}(t) = \bar{\eta}_w(t) - \bar{\eta}_e(t), \tag{5}$$

where $\bar{\eta}_w$ and $\bar{\eta}_e$ are the mean of sea level from tide gauges (1,2,3) and (6,7,8), respectively (Figure 2).

The time variation of $I_{\Delta\eta}$ is shown in Figure 9a. The middle row shows the mean surface circulation conditioned on $I_{\Delta\eta}$. More specifically, Figure 9b shows the mean surface circulation when $I_{\Delta\eta}$ is in the top third of its distribution (i.e., above the second tercile). Figure 9c is the mean circulation when $I_{\Delta\eta}$ is in the bottom third of the distribution (i.e., below the first tercile). The bottom row shows coastal sea level, and $\eta^{\tau}+\eta^{F_b}+\eta^{d}$, conditioned on $I_{\Delta\eta}$ as for the circulation.

When $I_{\Delta\eta}$ is high, the flow along the coast of Japan is weak to the west of 136°E. East of this longitude a relatively strong alongshore flow is seen along the coast. The impact of these changes in coastal current is

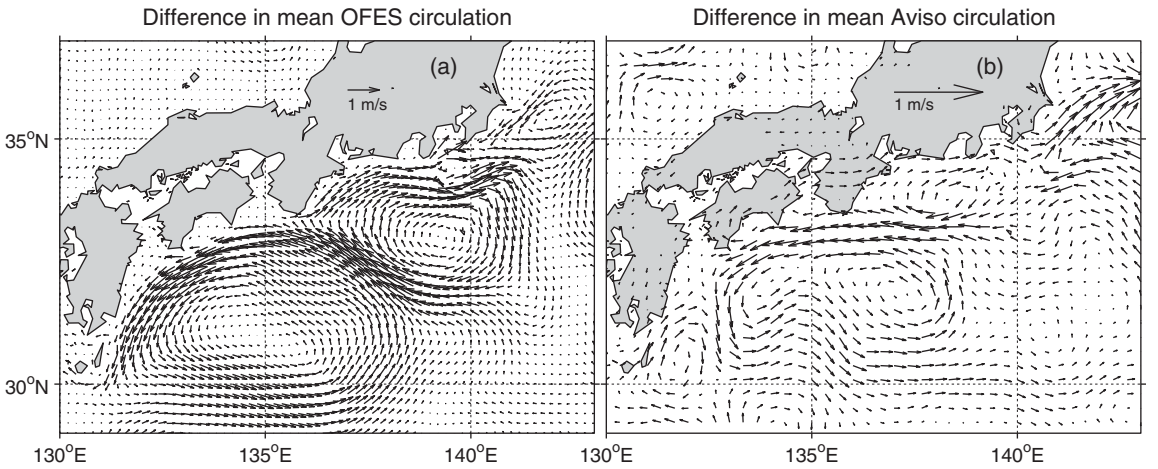

Figure 10. Difference in mean surface circulation when the sea level tilt index $I_{\Delta\eta}$ is relatively high and low (see text for details). (a) Surface circulation difference predicted by OFES (Figure 9b–9c). (b) Absolute geostrophic velocity difference based on altimeter observations. The data were obtained from Archiving, Validation and Interpretation of Satellite Oceanographic data (Aviso), published in September 2010. The weekly velocities were averaged into monthly values to align them with the monthly values of $I_{\Delta\eta}$.

reflected in the alongshore tilt profile (Figure 9d). The combined effect of bottom friction associated with the stronger nearshore flow, and a decrease in η^d due to an increase in the nearshore density, leads to the relatively large tilt east of 136°E. When $I_{\Delta\eta}$ is low, the Kuroshio has a well-defined, large meander. The flow west of 136°E is now stronger but there is no nearshore flow east of this longitude. For this case, the influence of η^d is small and the main contribution to the alongshore sea level tilt west of 136°E is due to bottom friction acting on the nearshore flow (Figure 9e).

The difference in the conditional means of surface circulation for high and low $I_{\Delta\eta}$ (Figures 9b–9c) is shown in Figure 10a. To test the realism of this circulation pattern, we calculated the difference in conditional means of absolute geostrophic velocity inferred from altimeter observations using the same conditional averaging approach (Figure 10b). The large-scale features of the two difference patterns are quite similar, providing support for the realism of the OFES predictions of surface circulation in this region.

The main conclusion we draw from these conditional means is that the tilt of sea level along the south coast of Japan is influenced strongly by the Kuroshio Current and, in particular its offshore position: the strongest tilts are detected when the Kuroshio Current is close to shore, east of about 136°E, where the shelf is relatively narrow; when the Kuroshio Current is close to the shore west of 136°E its effect on the coastal currents is more limited, presumably because the shelf is wider. Assuming these results hold at zero frequency (i.e., for the long-term mean), we then speculate that the coastal mean tilt shown in Figure 2 is due to nearshore circulation, driven by the Kuroshio Current when it is close to shore.

5. Summary and Discussion

The tilt of coastal mean sea level along the Pacific coast of Japan and the west coast of the US and Canada has been estimated using two independent approaches. The geodetic approach is based on tide gauge observations, GPS measurements at gauge reference marks and a geoid model. The ocean approach uses a high-resolution, dynamically based ocean model. Along the west coast of North America, both approaches give similar large-scale profiles with a minimum at about 40°N and a maximum in the northern part of the Gulf of Alaska. The range in the large-scale signal, which spans more than 20° of latitude, is about 20 cm for the geodetic approach and 14 cm for the ocean approach. Along the Pacific coast of Japan, both approaches predict an eastward sea level drop of about 20 cm along the south coast and a further northward drop in sea level across Tsugaru Strait consistent with the observed mean eastward flow. The correlation between the geodetic and ocean profiles is 0.63 and 0.80 for North American and Japanese coast, respectively.

Differences in the colocated geodetic and ocean estimates at the North American gauges have a standard deviation of σ_{G-O}=8.0 cm. The spatial autocorrelation of the difference profile indicates the differences are effectively uncorrelated between tide gauges and, in this sense, small scale. Similar calculations for Japan gave differences in geodetic and ocean estimates with a standard deviation of 8.0 cm.

To understand the physical causes of the sea level tilts with respect to the geoid along both coasts, and also explain the differences in the estimates from the two approaches, the alongshore momentum balance was integrated along each coast to decompose the signal predicted by the OFES into components due to local wind stress, friction, and water density. Along the North American coast, it was concluded that wind acting along the shelf was the primary driver of the mean sea level variability and, in accord with *Hickey and Pola* [1983], its effect could be described quite well using the arrested topographic wave theory of *Csanady* [1978]. (Visual inspection of the mean surface flow field over the eastern North Pacific confirmed the existence of a coastal boundary layer, decoupled from the large-scale circulation of the adjacent open ocean.) Along the south coast of Japan the local wind makes a negligible contribution to the tilt. Based on composites of OFES circulation conditioned on coastal sea level differences, we speculate that the Kuroshio, through its effect on coastal circulation, is the primary driver of the tilt.

What causes the differences in MDT profiles predicted by the two approaches? Assume the variance of the difference in profiles can be approximated by $\sigma^2_{G-O}=\sigma^2_g+\sigma^2_o$ where σ_g and σ_o are the standard deviation of the errors of the geodetic and ocean estimates, assumed uncorrelated. *Kuroishi* [2009] compared geoid heights based on JGEOID2008 and GPS/leveling and found the standard deviation of the discrepancies to be 8.4 cm. *Kuroishi* [2009] also found that the discrepancies were influenced by a large wavelength error that was attributed to errors in the foundational geopotential model. *Kuroishi* [2009] statistically modeled the long wavelength error using a simple tilted plane and found its removal reduced the standard deviation of the GPS/leveling discrepancies from 8.4 to 6.0 cm. Correcting the geodetic profile for the long wavelength error reduces σ_{G-O} from 8.0 to 7.5 cm. If we assume σ_g=6.0 cm and σ_{G-O}=7.5 cm, we estimate the standard deviation of the ocean model errors to be $\sigma_o=\sqrt{7.5^2-6.0^2}$=4.5 cm. We conclude that the errors in the ocean model and geoid model, after correction for the long wavelength error, have approximately similar magnitudes along the Pacific coast of Japan. For the North American coast, the estimated error for the CGG2013 geoid heights ranges between 1.6 and 5.9 cm and, as mentioned above, comparison of CGG2013 to GPS/leveling data gives a standard deviation of 4.4 cm. This is too small to explain the differences in the geodetic and ocean estimates for the North American coast and we infer $\sigma_o=\sqrt{8.0^2-4.4^2}$=6.7 cm. Part of the explanation for this error lies in the limited horizontal resolution of the ocean model. For example, a simple wind setup calculation shows that local changes in the wind field and orientation of the coastline could cause sea level changes of several cm over the width of one ocean model grid cell. The ocean model also excludes physical processes that may cause localized variations in mean sea level of several cm, e.g., local inputs of freshwater, rectification of the tides, and wave setup. We conclude that the difference in the geodetic and ocean estimates for the North American coast is due to a combination of ocean and geoid model errors with most of the error coming from the ocean models.

One obvious next step is to use higher-resolution regional models to downscale results from global ocean models like OFES to the coast. Grid spacing of order 1 km will be required to accurately predict the penetration of deep ocean signals across the continental slope and shelf, and the contribution of poorly resolved phenomena (e.g., the arrested topographic wave) and missing shelf processes such as those mentioned above. A high-resolution ocean model could also be used to perform sensitivity studies in order to better understand the dynamics controlling the coastal tilts. For example, it could be used to explain why different values of σ had to be specified in (2) to balance the alongshore momentum equation (1) along each coast and the role of friction in general. The high-resolution model could also be used to better understand how the Kuroshio drives nearshore circulation along the south coast of Japan. For the geodetic estimates, these can be potentially improved by including Release 5 GOCE data in the regional geoid models. (Note CGG2013 uses GOCE information that is approximately equivalent to spherical harmonic degree and order 150, corresponding to a spatial resolution of 133 km.) Furthermore, the North America geoid models could also be improved by integrating the new US airborne gravity data (GRAV-D project) available along the Pacific coast.

Acknowledgments
We thank Yuki Kuroishi for kindly providing geoid heights at the Japanese tide gauges. We also thank Phil Woodworth and Simon Higginson for useful discussions. We appreciate comments from the Editor and two anonymous reviewers that improved an earlier version of the manuscript. The mean dynamic topographies (MDT) used to generate Figures 1 and 2 are listed in Tables 1 and 2. The geodetic MDT estimates for the Pacific coast of North America were provided by our coauthors from Natural Resources Canada (Jianliang.Huang@NRCan-RNCan.gc.ca; Marc.Veronneau@NRCan-RNCan.gc.ca). The CESM model output was provided by Yu-heng Tseng (ytseng@ucar.edu). All other data are described, and can be accessed via the links provided, in the Data and Methods section. H.L. acknowledges financial support from the Natural Science Foundation of China through contract U1405233, and the China Scholarship Council, to support his visit to Dalhousie University. K.R.T. acknowledges financial support from the Discovery Grant program of the Natural Science and Engineering Research Council of Canada.

References

Andersen, O. B. (2010), The DTU10 gravity field and mean sea surface, paper presented at Second International Symposium of the Gravity Field of the Earth (IGFS2), International Association of Geodesy (IAG), Fairbanks, Alaska.
Andersen, O. B., P. Knudsen, and P. A. Berry (2010), The DNSC08GRA global marine gravity field from double retracked satellite altimetry, *J. Geod.*, *84*(3), 191–199.
Craymer, M., J. Henton, M. Piraszewski, and E. Lapelle (2011), An updated GPS velocity field for Canada, Abstract G21A-0793 presented at 2011 Fall Meeting, AGU, San Francisco, Calif., 5–9 Dec.
Csanady, G. T. (1978), The arrested topographic wave, *J. Phys. Oceanogr.*, *8*(1), 47–62.
Csanady, G. T. (1982), *Circulation in the Coastal Ocean*, vol. 2, 279 pp., Springer, Netherlands.
Daley, R. (1993), *Atmospheric Data Analysis*, 457 pp., Cambridge Univ. Press, Cambridge.
Ekman, M. (1989), Impacts of geodynamic phenomena on systems for height and gravity, *Bull. Géod.*, *63*(3), 281–296.
Featherstone, W. E., and M. S. Filmer (2012), The north-south tilt in the Australian height datum is explained by the ocean's mean dynamic topography, *J. Geophys. Res.*, *117*, C08035, doi:10.1029/2012JC007974.
Förste, C., et al. (2013), EIGEN-6C3stat—The Newest High Resolution Global Combined Gravity Field Model Based on the 4th Release of the GOCE Direct Approach. [Available at http://icgem.gfz-potsdam.de/ICGEM/documents/Foerste-et-al-EIGEN-6C3stat.pdf.]
Hickey, B. M., and N. E. Pola (1983), The seasonal alongshore pressure gradient on the west coast of the United States, *J. Geophys. Res.*, *88*(C12), 7623–7633.
Higginson, S., K. R. Thompson, P. L. Woodworth, and C. W. Hughes (2015), The tilt of mean sea level along the east coast of North America, *Geophys. Res. Lett.*, *42*, 1471–1479, doi:10.1002/2015GL063186.
Huang, J., and M. Véronneau (2013), Canadian gravimetric geoid model 2010, *J. Geod.*, *87*(8), 771–790.
Huthnance, J. M. (2004), Ocean-to-shelf signal transmission: A parameter study, *J. Geophys. Res.*, *109*, C12029, doi:10.1029/2004JC002358.
Ito, T., O. Togawa, M. Ohnishi, Y. Isoda, T. Nakayama, S. Shima, H. Kuroda, M. Iwahashi, and C. Sato (2003), Variation of velocity and volume transport of the Tsugaru Warm Current in the winter of 1999–2000, *Geophys. Res. Lett.*, *30*(13), 1678, doi:10.1029/2003GL017522.
Kalnay, E., et al. (1996), The NCEP/NCAR 40-year reanalysis project, *Bull. Am. Meteorol. Soc.*, *77*(3), 437–471.
Kuroishi, Y. (2009), Improved geoid model determination for Japan from GRACE and a regional gravity field model, *Earth Planets Space*, *61*(7), 807–813.
Kuroishi, Y. (2013), Comparison of latest global and regional gravimetric geoid models with GPS/leveling geoidal undulations over Japan, in *Reference Frames for Applications in Geosciences*, edited by Z. Altamimi, and X. Collilieux, pp. 221–227, Springer, Berlin, Heidelberg.
Kuroishi, Y., and W. Keller (2005), Wavelet approach to improvement of gravity field–geoid modeling for Japan, *J. Geophys. Res.*, *110*, B03402, doi:10.1029/2004JB003371.
Menéndez, M., and P. L. Woodworth (2010), Changes in extreme high water levels based on a quasi-global tide-gauge data set, *J. Geophys. Res.*, *115*, C10011, doi:10.1029/2009JC005997.
Pacanowski, R. C., and S. M. Griffies (1998), MOM 3.0 manual, technical report, Geophys. Fluid Dyn. Lab./NOAA, GFDL Ocean Group Technical Report No. 4, Princeton, N. J.
Pavlis, N. K., S. A. Holmes, S. C. Kenyon, and J. K. Factor (2012), The development and evaluation of the Earth Gravitational Model 2008 (EGM2008), *J. Geophys. Res.*, *117*, B04406, doi:10.1029/2011JB008916.
Pavlis, N. K., S. A. Holmes, S. C. Kenyon, and J. K. Factor (2013), Correction to "the development and evaluation of the Earth Gravitational Model 2008 (EGM2008)," *J. Geophys. Res. Solid Earth*, *118*, 2633, doi:10.1002/jgrb.50167.
Pedlosky, J. (1987), *Geophysical Fluid Dynamics*, 710 pp., Springer, N. Y.
Penna, N., W. Featherstone, J. Gazeaux, and R. Bingham (2013), The apparent British sea slope is caused by systematic errors in the leveling-based vertical datum, *Geophys. J. Int.*, *194*(2), 772–786.
Pugh, D., and P. Woodworth (2014), *Sea-Level Science: Understanding Tides, Surges, Tsunamis and Mean Sea-Level Changes*, 407 pp., Cambridge Univ. Press, Cambridge.
Saha, S., et al. (2010), The NCEP climate forecast system reanalysis, *Bull. Am. Meteorol. Soc.*, *91*(8), 1015–1057.
Santamaría-Gómez, A., M. Gravelle, X. Collilieux, M. Guichard, B. M. Míguez, P. Tiphaneau, and G. Wöppelmann (2012), Mitigating the effects of vertical land motion in tide gauge records using a state-of-the-art GPS velocity field, *Global Planet. Change*, *98*, 6–17.
Sasaki, H., M. Nonaka, Y. Masumoto, Y. Sasai, H. Uehara, and H. Sakuma (2008), An eddy-resolving hindcast simulation of the quasiglobal ocean from 1950 to 2003 on the Earth Simulator, in *High Resolution Numerical Modelling of the Atmosphere and Ocean*, edited by K. Hamilton, and W. Ohfuchi, pp. 157–185, Springer, N. Y.
Small, R. J., et al. (2014), A new synoptic scale resolving global climate simulation using the Community Earth System Model, *J. Adv. Model. Earth Syst.*, *6*, 1065–1094, doi:10.1002/2014MS000363.
Woodworth, P. L., and R. Player (2003), The permanent service for mean sea level: An update to the 21st century, *J. Coastal Res.*, *19*(2), 287–295.
Woodworth, P. L., C. W. Hughes, R. J. Bingham, and T. Gruber (2012), Towards worldwide height system unification using ocean information, *J. Geod. Sci.*, *2*(4), 302–318.
Wright, D. G., and K. R. Thompson (1983), Time-averaged forms of the nonlinear stress law, *J. Phys. Oceanogr.*, *13*(2), 341–345.
Xu, F.-H., and L.-Y. Oey (2011), The origin of along-shelf pressure gradient in the Middle Atlantic Bight, *J. Phys. Oceanogr.*, *41*(9), 1720–1740.